Acoustic Performance of Additively Manufactured Titanium Perforated Panels

Arun Arjunan[1, a *], Ahmad Baroutaji[1, b], Ahmad Latif[1, c], Mark Stanford[1, d], Ayyapan S. Praveen[2, e], Chang J. Wang[3, f], Kawa Manmi[4, 5, g] and Abdul G. Olabi[6, 7, h]

[1]School of Engineering, University of Wolverhampton, Telford Innovation Campus, TF2 9NT, UK
[2]Vel Tech Rangarajan Dr. Sagunthala R&D Institute of Science and Technology, Tamil Nadu, India
[3]Dept. of Engineering and Design, University of Sussex, Brighton BN1 9RH, UK
[4]School of Mathematics, University of Birmingham, B15 2TT, UK
[5] Dept. of Mathematics, College of Science, Salahaddin University-Erbil, Iraq
[6]Dept. of Sustainable and Renewable Energy Engineering, University of Sharjah, Sharjah, UAE
[7]School of Engineering and Applied Science, Aston University, Birmingham B4 7ET, UK

[a *]a.arjunan@wlv.ac.uk, [b] A.Baroutaji@wlv.ac.uk, [c]a.latif@wlv.ac.uk, [d]M.Stanford@wlv.ac.uk, [e]draspraveen@veltechuniv.edu.in, [f]C.J.Wang@sussex.ac.uk, [g]K.M.A.Manmi@bham.ac.uk, [h]aolabi@sharjah.ac.ae

Keywords: Titanium alloy; additive manufacturing; selective laser melting; sound transmission; sound absorption; micro-perforated panel.

Abstract Additively manufactured (AM) titanium products are increasingly being used in the aerospace industry where the acoustic-mechanical performance is of importance. However, the acoustic performance of AM Ti6Al4V and Ti6Al4V ELI (Extra Low Interstitial) has received limited attention in literature. Accordingly, this study investigates the sound absorption coefficient (α) and Sound Transmission Loss (STL) of both Ti6Al4V and Ti6Al4V ELI samples manufactured using Selective Laser Melting (SLM). Furthermore, the potential of developing Ti6Al4V alternatively shaped micro-perforated panels (MPP) within a frequency range of 400 to 1600 Hz is also explored.

1. Introduction

Lightweight structures that combine high strength, energy absorption [1–4] and acoustic performance [5–12] are of interest to automotive, aerospace and the building sectors [13]. A recent review by Arjunan *et al.* [14] found that metallic foams have gained popularity as a potential contender in this aspect due to their favourable mechanical and vibroacoustic properties. However, metallic foams still cannot match the structural performance of their bulk counterparts [15–18]. Consequently, there is a requirement for alternative sound absorbers that not only feature excellent acoustic properties but also allows for good structural strength.

The theoretical principles that describe the acoustic properties of microperforated panels (MPPs) are well known [19,20]. Nevertheless, a broadband MPP with high α require microscopic perforations requiring the use of expensive machining techniques. The rise in AM techniques such as Selective Laser Melting (SLM) [21,22] allows the creation of complex perforations and waveguides [23,24]. However, studies on the acoustic performance of AM metal MPPs that feature high $\alpha_\rho$and STL are scarce. In any case, no study has reported the acoustic performance of non-circular perforations with the exception of slits. Accordingly, this study explores the potential of developing an AM Ti6Al4V non-circular MPP system that may have a potential impact on both $\alpha_\rho$and STL.

2. Material and methods

2.1. Non-circular micro-perforated panels (MPPs). Approximating an MPP as a porous frame, the acoustic effect can be attributed to the perforation rate or porosity (ϕ), flow resistivity (σ), perforation thickness (d) and the mounting conditions. An MPP backed by an air cavity of depth $L\rho$ can be approximated as a collection of Helmholtz resonators with an air cavity volume $V_{ca\rho}$, neck length $d_\rho$and neck aperture area $_{perf}$. The volume in this instance, can be linked to the back-cavity

depth L. Accordingly, the total input impedance of the perforated-air layer combination can be written as shown in Eq. (1):

$$Z_A = \left(\frac{2d}{r} + 4\frac{\varepsilon_e}{r}\right)\frac{R_s}{\phi} + \frac{1}{\phi}(2\varepsilon_e + d)j\omega_{\ 0} - j_{\ 0}c_0\cot(k_0 L) \tag{1}$$

For such a resonance-based system, the highest $\alpha\rho$corresponds to the frequency of maximum resonance. Therefore, following Atalla and Sgard, the first mode of resonance at low frequency can be expressed in terms of the perforation area ($_{perf}$) as shown in Eq. (2):

$$\omega = \sqrt{\frac{{c_0}^2\ _{perf_i}}{(2\varepsilon_e + d)V_{ca\rho}}} \tag{2}$$

where $_{perf}/V_{ca\rho}$ represents the ratio of the perforation area to the corresponding volume of the backing cavity and $\varepsilon_{e\rho}\approx\rho\varepsilon_0(1-1.14\sqrt{\phi})\rho$is the correction term accounting for the interaction between the perforation.

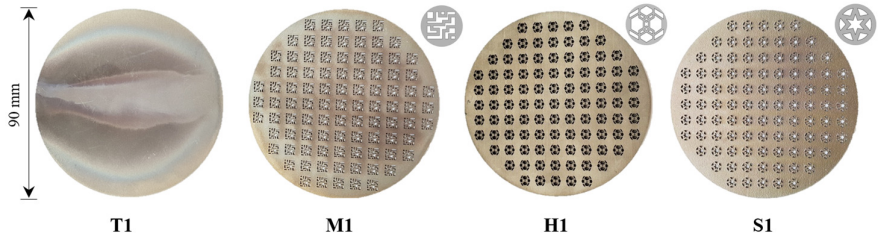

Fig. 1. Ti6Al4V MPP showing identifiers for solid (T1), maze (M1), hexagonal (H1) and star (S1) design.

Accordingly, keeping the $_{perf\rho}\approx 2.54\times10^{-6\rho}m^{2\rho}$ as a constant, three different perforation shapes (M1, H1 and S1) were designed as shown in Fig. 1. However, the ratio of the small to large area ($_s/\rho_{\ l}$) within a perforation is 0.6, 0.3 and 0.15 for S1, M1 and H1 respectively. An additional design T1 was also conceived and made of fully dense Ti6Al4V. This was used as the control specimen to characterise the acoustic performance of the AM material. The thickness (d) and diameter (D) of the panel used are 1 and 90 mm respectively. For designs M1, H1, and S1, two cases were considered: case 1 with (Fig. 2a) and case 2 without (Fig. 2b) a porous foam backing. In order to minimise airgaps and to ensure repeatability, the assemblies are made inside a holder as shown in Fig. 2c. A summary of the properties and the test designs are listed in Table 1.

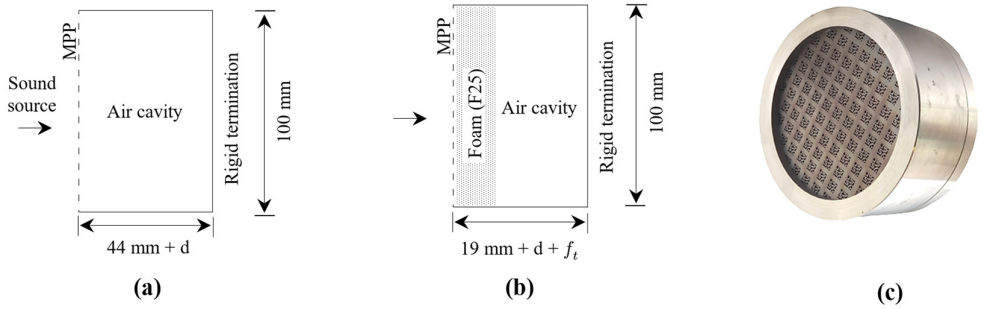

Fig. 2. Test cases considered where (a) MPP backed by 44 mm air cavity, (b) MPP backed by 25 mm foam and 19 mm air cavity and (c) MPP holder and test assembly used.

2.2. Additive manufacturing. All the MPPs were manufactured using an EOS M290 SLM machine at a 30 μm layer thickness. Ti6Al4V and Ti6Al4V ELI with a density of 4430 Kg/m^3 was the material of choice.

Table 1. Properties of the designs and materials considered.

Design	Thickness (mm)	Foam placement	$\sigma^{perf.}$ (10^{-6} m^2)	s/l	L (mm)
T1	1	-	-	-	44
F25	25	-	-	-	20
S1, M1, H1	1	-	2.54	0.6_{S1}, 0.3_{M1}, 0.15_{H1}	44
S1F25, M1F25, H1F25	1_{MPP}+25_{foam}	Back	2.54	0.6_{S1}, 0.3_{M1}, 0.15_{H1}	19
The flow resistivity of the perforated panel is 7312 Pa. s/m^2 and foam is 10900 Pa. s/m^2					
The tortuosity of the foam is ~1.					

2.3. Measurement of α and STL. α was characterised using an impedance tube-based transfer-function complying with ISO10534-2. An in-tube loudspeaker connected to a function generator via a PA50 power amplifier and a Fast Fourier Transform (FFT) spectrum analyser was used as the acoustic exciter. The STL measurements were carried out using a 4-microphone setup. The test setup considered two microphones (M1 and M2) which were mounted in the source chamber (SC) and other two microphones (M3 and M4) in the receiving chamber (RC).

3. Results and discussion

3.1. Acoustic performance of non-perforated Ti6Al4V. For Ti6Al4V, an α curve representative of non-porous hard metals can be observed as shown in Fig. 3a. The highest absorption was observed at 500 Hz namely 0.15 and 0.14 for Ti6Al4V and Ti6Al4V ELI respectively. This showed that approximately ~85-86% of the sound energy is reflected without penetrating the surface of the material. According both Ti6Al4V and ELI variant manufactured using SLM are fully dense resulting in a poor acoustic behaviour similar to other dense hard metals such as steel.

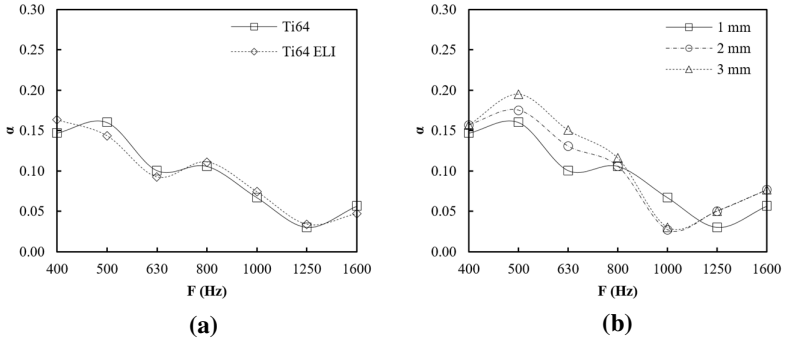

Fig. 3. sound absorption coefficient measured for (a) 1 mm Ti6Al4V and Ti6Al4V ELI flat specimens manufactured using SLM and (b) showing the influence of material thickness.

The performance difference between Ti6Al4V and Ti6Al4V ELI was found to be negligible. Consequently, further tests are limited to Ti6Al4V alone as the performance can be considered similar to Ti6Al4V ELI. Nevertheless, the relatively high α at low frequencies (400 to 800 Hz) can be attributed to the 1 mm sample thickness and the 44 mm airgap. This means that at low frequencies the sample can act as a baffle transferring the vibro-acoustic energy providing some damping.

Analysing the influence of material thickness as shown in Fig. 3b, a slight increase in α at the low frequencies due to a shift in resonance frequency as a result of the added mass can be observed. The highest improvement of ~0.05 was found at the highest thickness of 3 mm at 630 Hz in comparison to 1 mm. While certain differences can be observed in the α peaks between the material thickness tested, overall sound absorption remained poor despite the increased material thickness. Nevertheless, the results establish that the overall accuracy of α depends on the material thickness. Consequently, this study shows that fully dense SLM Ti6Al4V do not contribute significantly to α. The STL results (Fig. 4a) show that fully dense Ti6Al4V is excellent at resisting sound transmission and hence has a high STL. As a general rule, the higher the STL curve the better the acoustic isolation. Furthermore,

the material thickness has a substantial impact on the STL curves. The highest rate of improvement (+5 dB *avg.*) was observed when the thickness was increased from 1 mm to 2 mm. Even though the performance further increased at 3 mm, the rate of improvement was limited to +3 dB *avg*. The improvement in STL due to thickness observed can be primarily attributed to the increase in mass and can be related using Eq. (3), where f is the frequency and m'' is the mass per unit area.

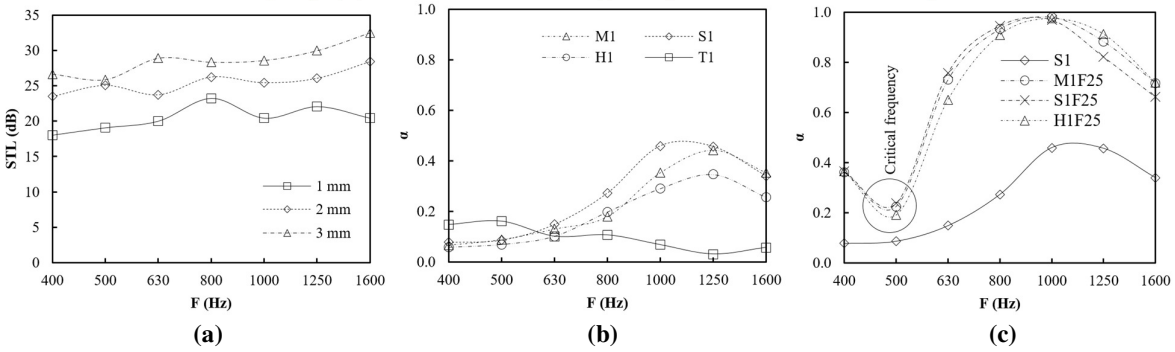

Fig. 4. Influence of (a) material thickness on the STL of Ti6Al4V, (b) Ti6Al4V non-circular MPP designs with a 44 mm back cavity and (c) α for micro-perforated Ti6Al4V panels featuring a 25 mm porous layer.

$$STL_f \approx 20 \log 10\ (fm'') - 47 \tag{3}$$

3.2. Ti6Al4V micro-perforated panel. Fig. 4b shows that the micro-perforations have a significant impact on the performance with α improving for majority of the frequencies (630-1600 Hz). However, a 10% decrease in performance was observed at the lowest frequency (400-630 Hz) tested. While the performance of all the designs show a similar trend, the best performance was exhibited by the design S1 followed by M1 and then H1.

It can be seen that the shape of perforation had a significant effect on the frequency of maximum α. The design S1 was found to match closely with the theoretical frequency which can be attributed area ratio ($_s/\rho_l$). The design S1, M1 and H1 featured a $_s/\rho_{l\rho}$ values of 0.6, 0.3 and 0.15 respectively. Therefore, in order to use the perforation area instead of diameter in the equivalent fluid model, the ratio of perforations ($_s/\rho_l$) has to be greater than 0.5. For the design H1 and M1, the peak absorption was observed at 1250 Hz as opposed to the design frequency of 1000 Hz. The best performance was observed for S1 again reiterating the importance of the $_s/\rho_l$. The highest absorption despite sharing the same perforation area was observed for the highest $_s/\rho_l$.

Even though the MPPs can be seen to improve α, best performances (25 to 30% improvement) were observed at f at or above 100 Hz. This is because of the inherent disadvantage demonstrated by the MPPs in suppressing the low-frequency noise (*i.e.* <1000 Hz) despite the optimal perforation area. In order to solve this problem, the layer interaction effect is exploited by coupling a 25 mm porous media to the highly stiff and reflective Ti6Al4V MPP layer backed up by a 19 mm air cavity.

Analysing Fig. 4c, the addition of a porous layer significantly increases α in comparison to all other cases considered. The improvement can be primarily attributed to the interaction effect caused due to the constitutive parameters, importantly the ratio of porosity and stiffness between the MPP and porous medium. The contribution of the interaction effect to α is so significant that complete absorption was observed at a frequency range of 800-1250 Hz with the overall performance following a quadratic curve. However, the improvement in α towards the lower frequency is limited by the critical frequency (f_c= 500 Hz) which is the first eigenmode frequency of the system. Overall, the interaction effects of the hybrid system featuring both the MPP and the porous layer outperforms the case that of the MPP that feature only the back-cavity. The MPP by itself feature relatively large perforation and Ti6Al4V inherently possess high structural strength and reflectivity. The foam on the other hand offers a high porosity though it is structurally weak. However, the combination is acoustically effective for enhanced sound absorption (Fig. 4c).

4. Conclusion

Complex perforation in high strength metals such as Ti6Al4V, which can be coupled with a porous medium to develop high-efficiency sound absorbers is demonstrated in this study. It was found that the as-manufactured Ti6Al4V and Ti6Al4V ELI using optimum SLM parameters is a poor sound absorber and reflects ~85-86% of the sound. In addition, the ELI variant did not show any significant difference in sound absorption when compared normal Ti6Al4V. While the influence of material thickness on $\alpha\rho$was found to be limited to 0.05_{α}, the highest material thickness (3 mm) exhibited the highest $\alpha\rho$(~0.18 *avg.*) at a frequency range of 400-800 Hz. When it comes to STL, fully dense Ti6Al4V showed excellent performance with a +5 dB (*avg.*) increase on doubling the thickness. The superior STL can be attributed primarily to the increase in mass following a trend that can be expressed as $20\log 10\rho(fm'') - 47$. The result of the novel Ti6Al4V+foam MPP developed in this study shows significant improvement in $\alpha\rho$at all frequencies above the critical frequency (f_c). The high $\alpha\rho$is the result of interaction effect between the MPP and the porous layer. Lastly, it is demonstrated that for non-circular perforation, the perforation area can be used in the equivalent fluid model to predict the peak absorption frequency. The study further validates that the perforations can be of any shape and not necessarily circular to obtain high $\alpha\rho$values.

References

[1] A. Baroutaji, M.D. Gilchrist, D. Smyth, A.G. Olabi, Analysis and optimization of sandwich tubes energy absorbers under lateral loading, Int. J. Impact Eng. 82 (2015) 74–88. doi:10.1016/j.ijimpeng.2015.01.005.

[2] A. Baroutaji, E. Morris, A.G. Olabi, Quasi-static response and multi-objective crashworthiness optimization of oblong tube under lateral loading, Thin-Walled Struct. 82 (2014) 262–277. doi:10.1016/j.tws.2014.03.012.

[3] A. Baroutaji, M. Sajjia, A.-G.A.-G. Olabi, On the crashworthiness performance of thin-walled energy absorbers: Recent advances and future developments, Thin-Walled Struct. 118 (2017) 137–163. doi:10.1016/j.tws.2017.05.018.

[4] A. Baroutaji, A. Arjunan, A. Niknejad, T. Tran, A.-G. Olabi, Application of Cellular Material in Crashworthiness Applications: An Overview, in: Ref. Modul. Mater. Sci. Mater. Eng., Elsevier, 2019. doi:10.1016/B978-0-12-803581-8.09268-7.

[5] A. Arjunan, C. Wang, M. English, M. Stanford, P. Lister, A computationally-efficient numerical model to characterize the noise behavior of metal-framed walls, Metals (Basel). 5 (2015) 1414–1431. doi:10.3390/met5031414.

[6] A. Arjunan, C.J. Wang, K. Yahiaoui, D.J. Mynors, T. Morgan, V.B. Nguyen, M. English, Development of a 3D finite element acoustic model to predict the sound reduction index of stud based double-leaf walls, J. Sound Vib. 333 (2014) 6140–6155. doi:10.1016/j.jsv.2014.06.032.

[7] A. Arjunan, C.J. Wang, K. Yahiaoui, D.J. Mynors, T. Morgan, M. English, Finite element acoustic analysis of a steel stud based double-leaf wall, Build. Environ. 67 (2013) 202–210. doi:10.1016/j.buildenv.2013.05.021.

[8] A. Arjunan, Noise emission levels associated with the 2016 UWR Formula 3 Car and the influence of an aftermarket silencer end cap, in: INTER-NOISE 2017 - 46th Int. Congr. Expo. Noise Control Eng. Taming Noise Mov. Quiet, 2017.

[9] A. Arjunan, C.J. Wang, K. Yahiaoui, D.J. Mynors, T. Morgan, V.B. Nguyen, M. English, Sound frequency dependent mesh modelling to simulate the acoustic insulation of stud based double-leaf walls, in: Proc. ISMA 2014 - Int. Conf. Noise Vib. Eng. USD 2014 - Int. Conf. Uncertain. Struct. Dyn., 2014.

[10] A. Arjunan, Sound transmission loss of light-weight slotted steel studs in a gypsum plasterboard partition wall, in: Proc. INTER-NOISE 2016 - 45th Int. Congr. Expo. Noise Control Eng. Towar. a Quieter Futur., 2016.

[11] A. Arjunan, A. Foteinou, A comparative study on the acoustic behaviour of free-standing curved and flat single panel screens in an open-plan enclosed environment, in: INTER-NOISE 2017 - 46th Int. Congr. Expo. Noise Control Eng. Taming Noise Mov. Quiet, 2017.

[12] A. Arjunan, J. Rackley, M. Stanford, Experimental investigation on the sound reduction performance of frequency controlled acoustic interference cavities, in: Proc. INTER-NOISE 2016 - 45th Int. Congr. Expo. Noise Control Eng. Towar. a Quieter Futur., 2016.

[13] A. Arjunan, C.J. Wang, D.J. Mynors, K. Yahiaoui, Thermal efficiency analysis of slotted steel studs in double leaf partition walls using FEM and experimental tests, 2013.

[14] A. Arjunan, A. Baroutaji, A.S. Praveen, A.G. Olabi, C.J. Wang, Acoustic Performance of Metallic Foams, in: Ref. Modul. Mater. Sci. Mater. Eng., Elsevier, 2019. doi:10.1016/B978-0-12-803581-8.11561-9.

[15] K. Bari, A. Arjunan, Extra low interstitial titanium based fully porous morphological bone scaffolds manufactured using selective laser melting, J. Mech. Behav. Biomed. Mater. 95 (2019) 1–12. doi:10.1016/j.jmbbm.2019.03.025.

[16] A. Vance, K. Bari, A. Arjunan, Compressive performance of an arbitrary stiffness matched anatomical Ti64 implant manufactured using Direct Metal Laser Sintering, Mater. Des. 160 (2018) 1281–1294. doi:10.1016/j.matdes.2018.11.005.

[17] A. Vance, K. Bari, A. Arjunan, Investigation of Ti64 sheathed cellular anatomical structure as a tibia implant, Biomed. Phys. Eng. Express. 5 (2019) 035008. doi:10.1088/2057-1976/ab0bd7.

[18] A.S. Praveen, A. Arjunan, Parametric optimisation of High-Velocity Oxy-Fuel Nickel-Chromium-Silicon-Boron and Aluminium-Oxide coating to improve erosion wear resistance, Mater. Res. Express. (2019). doi:10.1088/2053-1591/ab301c.

[19] S. Ortiz, C. Gonzalez, P. Cobo, F. Montero de Espinosa, Attenuating open cavity tones by lining its walls with microperforated panels, Noise Control Eng. J. 62 (2014) 145–151. doi:10.3397/1/376215.

[20] J. Pfretzschner, P. Cobo, F. Simón, M. Cuesta, A. Fernández, Microperforated insertion units: An alternative strategy to design microperforated panels, Appl. Acoust. 67 (2006) 62–73. doi:10.1016/j.apacoust.2005.05.005.

[21] S. Greiner, K. Wudy, L. Lanzl, D. Drummer, Selective laser sintering of polymer blends: Bulk properties and process behavior, Polym. Test. 64 (2017) 136–144. doi:10.1016/j.polymertesting.2017.09.039.

[22] A. Arjunan, M. Demetriou, A. Baroutaji, C. Wang, Mechanical performance of highly permeable laser melted Ti6Al4V bone scaffolds, J. Mech. Behav. Biomed. Mater. 102 (2020). doi:10.1016/j.jmbbm.2019.103517.

[23] A. Arjunan, Acoustic absorption of passive destructive interference cavities, Mater. Today Commun. 19 (2019) 68–75. doi:10.1016/j.mtcomm.2018.12.012.

[24] A. Arjunan, Targeted sound attenuation capacity of 3D printed noise cancelling waveguides, Appl. Acoust. 151 (2019) 30–44. doi:10.1016/J.APACOUST.2019.03.008.